



# Influence of anodizing variables on Cr(VI) photocatalytic reduction using TiO<sub>2</sub> nanotubes obtained by anodic oxidation

Anabela N. Dwojak<sup>a</sup>, María L. Vera<sup>a</sup>, Hernán D. Traid<sup>a</sup>, María F. Maydana<sup>a</sup>, Marta I. Litter<sup>b</sup>, Carlos E. Schvezov<sup>a,\*</sup>

<sup>a</sup> Instituto de Materiales de Misiones (IMAM) Universidad Nacional de Misiones, CONICET, Facultad de Ciencias Exactas Químicas y Naturales, Félix de Azara 1552, 3300 Posadas, Prov. de Misiones, Argentina

<sup>b</sup> Instituto de Investigación e Ingeniería Ambiental (IIIA), Universidad Nacional de San Martín, CONICET, Campus Miguelete, Av. 25 de Mayo y Francia, 1650 San Martín, Prov. de Buenos Aires, Argentina

## ARTICLE INFO

### Keywords:

Nanostructures  
Surfaces  
Photocatalytic properties  
Anodic oxidation  
Hexavalent chromium reduction

## ABSTRACT

The effect of growth conditions of TiO<sub>2</sub> films with nanotubular structures produced by anodic oxidation in electrolytes containing NH<sub>4</sub>F in glycerol and water was investigated. The effect of anodizing voltage, time, NH<sub>4</sub>F concentration and initial surface preparation on the formation of nanotube arrays was evaluated. In these cases, the structure was characterized by using scanning electron microscopy, X-ray diffraction and UV-Vis diffuse reflectance spectroscopy. The photocatalytic activity was evaluated using hexavalent chromium in the presence of EDTA (EDTA/Cr(VI) = 1.25 M ratio). The results show that uniform nanotube arrays were only formed with an applied voltage of 20 V, independently of the value of the other parameters studied. The photocatalytic activity increases with the NH<sub>4</sub>F concentration and the anodizing time, due to the increase in the length of the nanotubes, achieving the highest Cr(VI) transformation (93.8%) after 5 h UV irradiation under the optimal conditions.

## 1. Introduction

Titanium dioxide (TiO<sub>2</sub>) is a semiconductor used in heterogeneous catalysis for disinfection and decontamination of water and air due to the highly reactive species produced under UV radiation, able of transforming chemical species to less toxic ones; even mineralization is possible (Malato et al., 2009). TiO<sub>2</sub> is widely used due to its low cost, biocompatibility, photostability, commercial availability, water stability and high photocatalytic efficiency. The decontamination processes usually use TiO<sub>2</sub> particles suspended in water, and their reuse requires the separation and recovery of the particles. These steps can be avoided by immobilizing the TiO<sub>2</sub> particles in supporting structures (Robert et al., 2013). However, immobilization generally leads to a reduction in the photocatalytic activity due to the decrease in contact surface area and limitations in mass transfer.

At present, the efforts on the use of TiO<sub>2</sub> in photocatalytic systems are focused on the production of one-dimensional nanostructures such as nanotubes, which present geometrical, optical, electronic and chemical advantages, permitting fast electron transport and low electron-hole recombination (Pang et al., 2014; Albu et al., 2008). TiO<sub>2</sub>

nanotube films prepared by anodic oxidation provide optical, electronic, chemical and mechanical advantages, whereby they become suitable for technological applications. These properties make them suitable for a wide range of applications such as heterogeneous photocatalysis and other fields as sensors, solar cells, hydrogen production, molecular filtration and controlled released of drugs (Grimes and Mor, 2009 and references therein). For photocatalytic applications, there is still the challenge of achieving a high surface area and photocatalytic activity combined with an adequate adhesion and mechanical resistance of the nanotubes, which would allow their reuse (Nakata and Fujishima, 2012).

Immobilized nanotube arrays are produced by different techniques, e.g., use of templates of nanoporous alumina, sol-gel transcription processes with organo-gelator templates, seeded growth mechanisms, and hydrothermal techniques (see e.g., Stodolny et al., 2017)). However, the anodic oxidation (Grimes and Mor, 2009; Pichat, 2014) through the use of fluoride ions (F<sup>-</sup>) in the electrolyte allows to obtain nanotubular TiO<sub>2</sub> structures as a result of the competition between the formation and dissolution of the anodic titania layer (see the supplementary information (SI), section S1, for the mechanism of nanotubes

\* Corresponding author.

E-mail address: [schvezov@gmail.com](mailto:schvezov@gmail.com) (C.E. Schvezov).

<https://doi.org/10.1016/j.enmm.2021.100537>

Received 11 March 2021; Received in revised form 16 June 2021; Accepted 28 July 2021

Available online 30 July 2021

2215-1532/© 2021 Elsevier B.V. All rights reserved.

array formation) (Gong et al., 2001; Wang et al., 2011). The electrolyte composition determines the production of different types of nanotubes: a 1st generation prepared in aqueous HF, with lengths up to 500 nm; a 2nd generation up to 5 mm long, grown in aqueous solutions of fluoride salts; and a 3rd generation of smoother and longer nanotubes, up to 100–1000  $\mu\text{m}$ , grown in organic electrolytes containing  $\text{F}^-$  and small amounts of water (0.1–5 wt%) (Regonini et al., 2013 and references therein). In addition, anodic oxidation is a low-cost technique and the dimensions of the nanotubes may be controlled by modifying process parameters such as applied voltage, current density and  $\text{F}^-$  concentration (Rudnev et al., 2004; Traid et al., 2017). In addition, the electrolyte composition determines the morphology of the nanotubes: organic based electrolytes allow to obtain longer nanotubes (up to 1000  $\mu\text{m}$ ) than inorganic ones (Vera et al., 2018).

The photocatalytic activity of the anodic nanotubes is usually determined by spectrophotometry, following the color degradation of a colorant added in the solution (Wang et al., 2007; Masahashi et al., 2009; Macak et al., 2007; Zeng et al., 2011). This technique is not conclusive since other process like photolysis, reduction or sensitization may occur simultaneously, preventing the determination of the pure effect of the photocatalyst on the degradation of the dye (Pichat, 2014; Yan et al., 2006; Ollis et al., 2015; Barbero and Vione, 2016).

The hexavalent chromium system in the presence of ethylenediaminetetraacetic acid (EDTA, Cr(VI)/EDTA) is a more reliable system. In this system, the reduction of Cr(VI) to Cr(III) in the presence of EDTA as a hole trap (sacrificial synergetic agent) has been proved to be very appropriate and simple. The photocatalytic activity is measured by following the evolution of the Cr(VI) concentration in solution. In addition, this method can provide a direct evaluation of decontamination of industrial effluents containing dangerous ions like Cr(VI), which is a human carcinogen, environmentally important due to its toxicity. On the other hand, the reduction product Cr(III) is considered nontoxic. For this reason, transformation of Cr(VI) to Cr(III) is the most used way to eliminate chromium from wastewaters (Chromium Compounds, 2005).

In the present research, nanotubular  $\text{TiO}_2$  arrays were produced by anodic oxidation of commercial titanium plates in glycerol based electrolytes. The effect of anodizing voltage, time,  $\text{NH}_4\text{F}$  concentration and initial surface preparation on the characteristics of the nanotube arrays was investigated. The structure and morphology of the nanotubes were characterized, and the photocatalytic activity was determined by following the Cr(VI) concentration in a Cr(VI)/EDTA solution. In addition, the reproducibility of the process was assessed as well as the reusability of the arrays.

## 2. Experimental

### 2.1. Materials and methods

All chemicals were reagent grade and used without further purification. Glycerol (Anedra, 99.9%), ethylene glycol (Cicarelli, 99%) ammonium fluoride ( $\text{NH}_4\text{F}$ , Biopack), potassium dichromate ( $\text{K}_2\text{Cr}_2\text{O}_7$ , Biopack), EDTA (Riedel de Haën AG, Seeelze – Hannover), diphenylcarbazide (DFC, Biopack), acetone (Biopack, 99.5%), isopropyl alcohol (Anedra, 99.5%), methanol, nitric acid ( $\text{HNO}_3$ , Anedra, 65%), hydrofluoric acid (HF, Biopack, 40%) and phosphoric acid ( $\text{H}_3\text{PO}_4$ , Anedra, 85%) were used. Deionized water (conductivity = 0.05–0.06  $\mu\text{S}\cdot\text{cm}^{-1}$ ) was produced with an Osmoion Apema equipment. All pH adjustments were made with perchloric acid (Sintorgan, 69–72%). For anodization, a JMB direct current (DC) source, model LPS360DD, was used. For measuring the UV light irradiance, a home-made Arduino-based radiometer (at  $\lambda = 365\text{ nm}$ ) was used. A UV-Vis spectrophotometer (Shimadzu, UV-2550) was used for spectrophotometric measurements. Scanning electron microscopy (SEM) was performed using Carl Zeiss FE-SEM Sigma and Supra 40 equipments. The micrographs were taken with 3 or 5 kV and magnifications between 40 kX and 100 kX with

**Table 1**  
Surface preparation of the substrate for anodizing (see SI, Section S2).

	Identification letter	Process
Substrate preparation	R	Roughing with CSI paper with decreasing grain size from #120 to #500.*
	P	Polished by manual roughing up to #1500 and polishing with 1 $\mu\text{m}$ diamond lubricated with ethylene glycol in a polishing machine.*
	C	Chemical pickling with $\text{HF}:\text{HNO}_3:\text{H}_2\text{O}$ 1:4:5 (Wang et al., 2012) for 2 min.
	D	Degreased in ultrasound with methanol, followed by isopropanol and acetone (10 min each reagent) (Wang and Chen, 2013).

\*For this process, the plate was included in PVC tubes and with an acrylic matrix for surface finishing.

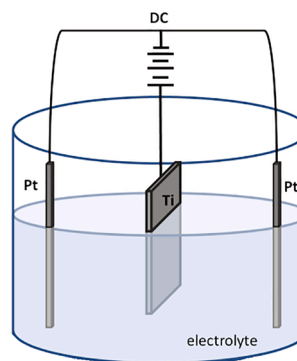


**Fig. 1.** Scheme of the anodic oxidation setup.

InLess detectors.

### 2.2. Photocatalyst preparation

The substrates for anodic oxidation were titanium square plates (Grade 2 according to ASTM B367), 4  $\text{cm}^2$  in area and 0.2 cm in thickness. Different surface preparations were made following the procedures shown in Table 1, to remove the natural oxide present on the substrate. Titanium plates were included in acrylic (Subiton) and abrasive papers mechanically polished with SiC (Koln) from #120 to #1500, followed by the use of 1  $\mu\text{m}$  diamond paste (Praxis) lubricated with ethylene glycol (Cicarelli) for 30 min in a homemade polishing machine (250 rpm). The surfaces were finally cleaned with water and detergent, and dried with hot air.

The titanium plates after the surface preparation were anodically oxidized at room temperature (RT) using a  $\text{NH}_4\text{F}$  solution as the electrolyte at one of the following concentrations: 0.27, 0.15 or 0.06 M in glycerol: water 1:1 at constant potentials in the range of 10 to 100 V during one of the following periods of time: 0.5, 1, 2 or 4 h. A DC was applied between two Pt sheets used as cathodes and a Ti anode, separated each other by 3 cm, as illustrated in Fig. 1. Both, applied voltage (V) and current density (J) were registered during oxidation. Immediately after oxidation, the samples were rinsed with demineralized water and dried with hot air. The samples with nanotubular films were thermally treated (TT) at 450  $^\circ\text{C}$  for 2 h with a heating ramp of 10  $^\circ\text{C}/\text{min}$  and cooling inside the furnace.

Samples were labeled as follows: a letter “G”, to identify the organic based electrolyte (glycerol); a number to indicate the  $\text{NH}_4\text{F}$  molar concentration (M); the applied voltage in volts (V); the oxidation time in hours (h); the specific surface preparation prior to oxidation (R, P, C or D, according to Table 1) and TT for the thermally treated samples. For instance, G-0.27M-20V-2h-C-TT indicates a sample oxidized in glycerol

**Table 2**Summary of the TiO<sub>2</sub> nanotube thin films preparation methodology. Characteristic dimensions and calculated bandgaps of the samples with nanotubular morphology.

Sample	Concentration NH <sub>4</sub> F [M]	Voltage [V]	Time [hours]	Surface preparation	Nanotubular morphology*	Di [nm]	L [nm]	W [nm]	E <sub>g</sub> [eV]
1 G-0.06M-20V-2h-C-TT	0.06	20	2	Chemical pickling	Yes	72 ± 15	700 ± 19	9 ± 2	3.31
2 G-0.06M-40 V-1 h-C	0.06	40	1	Chemical pickling	No	–	–	–	–
3 G-0.06M-40V-2h-C	0.06	40	2	Chemical pickling	No	–	–	–	–
4 G-0.06M-40 V-4 h-C	0.06	40	4	Chemical pickling	No	–	–	–	–
5 G-0.06M-60 V-1 h-C	0.06	60	1	Chemical pickling	No	–	–	–	–
6 G-0.06M-60V-2h-C	0.06	60	2	Chemical pickling	No	–	–	–	–
7 G-0.06M-60 V-4 h-C	0.06	60	4	Chemical pickling	No	–	–	–	–
8 G-0.06M-80V-2h-C	0.06	80	2	Chemical pickling	No	–	–	–	–
9 G-0.06M-100V-2h-C	0.06	100	2	Chemical pickling	No	–	–	–	–
10 G-0.15M-20V-2h-C-TT	0.15	20	2	Chemical pickling	Yes	70 ± 15	1154 <sup>†</sup>	8 ± 1	3.32
11 G-0.15M-40 V-1 h-C	0.15	40	1	Chemical pickling	No	–	–	–	–
12 G-0.15M-40V-2h-C	0.15	40	2	Chemical pickling	No	–	–	–	–
13 G-0.15M-40 V-4 h-C	0.15	40	4	Chemical pickling	No	–	–	–	–
14 G-0.15M-60 V-1 h-C	0.15	60	1	Chemical pickling	No	–	–	–	–
15 G-0.15M-60V-2h-C	0.15	60	2	Chemical pickling	No	–	–	–	–
16 G-0.15M-60 V-4 h-C	0.15	60	4	Chemical pickling	No	–	–	–	–
17 G-0.15M-80V-2h-C	0.15	80	2	Chemical pickling	No	–	–	–	–
18 G-0.15M-100V-2h-C	0.15	100	2	Chemical pickling	No	–	–	–	–
19 G-0.27M-10V-2h-P-TT	0.27	10	2	Polished	Yes	36 ± 6	–	6 ± 1	–
20 G-0.27M-20 V-0.5 h-C-TT	0.27	20	0.5	Chemical pickling	Yes	59 ± 15	915 ± 27	10 ± 2	3.33
21 G-0.27M-20 V-1 h-C-TT	0.27	20	1	Chemical pickling	Yes	72 ± 6	1144 ± 78	8 ± 1	3.32
22 G-0.27M-20V-2h-C-TT	0.27	20	2	Chemical pickling	Yes	61 ± 7	1760 ± 62	5 ± 1	3.30
23 G-0.27M-20V-2h-R-TT	0.27	20	2	Roughing	Yes	56 ± 1	~1760 <sup>†</sup>	8 ± 1	3.33
24 G-0.27M-20V-2h-D-TT	0.27	20	2	Degreased	Yes	68 ± 11	~1760 <sup>†</sup>	9 ± 1	3.32
25 G-0.27M-20V-2h-P-TT	0.27	20	2	Polished	Yes	61 ± 9	≥ 1760 <sup>†</sup>	9 ± 1	3.32
26 G-0.27M-30V-2h-C-TT	0.27	30	2	Polished	No	–	–	–	–
27 G-0.27M-40V-2h-C	0.27	40	2	Polished	No	–	–	–	–
28 G-0.27M-50V-2h-C	0.27	50	2	Polished	No	–	–	–	–
29 G-0.27M-60V-2h-C	0.27	60	2	Polished	No	–	–	–	–

<sup>†</sup> Not measured. Value estimated from measured values and oxidation conditions.

\* Presence of nanotubes in the TiO<sub>2</sub> coating.

with 0.27 M electrolyte concentration, at 20 V, during 2 h, of a substrate chemically treated with a post anodization TT. Table 2 shows the conditions under which all the coatings were synthesized.

The reproducibility of the anodizing process was evaluated repeating the whole anodizing procedure for G-0.27M-20V-2h-C-TT and G-0.27M-20V-2h-C-TT-d samples in independent experiments.

### 2.3. Characterization of the nanotubular coatings

Samples were analyzed by SEM and the analysis of the images was

made with the ImageJ software (Schneider et al., 2012); the average inner diameter (*Di*) and the wall thickness (*W*) of the nanotubes were determined as the average of 50 measurements in the SEM micrographs, on the top view of the nanotubes. The lengths (*L*) were measured on cross-sectional SEM views of nanotubes obtained by scratching the coating with a pin that made the nanotubes detach from the arrangement and fall down. For glancing incidence X-ray diffraction (GI-XRD), a Rigaku diffractometer model Smartlab SE with a D/teX Ultra 250 detector was used with CuK $\alpha$  radiation at a 0.02 (2 $\theta$ /s) scan rate and a 1° glancing angle. The accelerating voltage and the applied current were

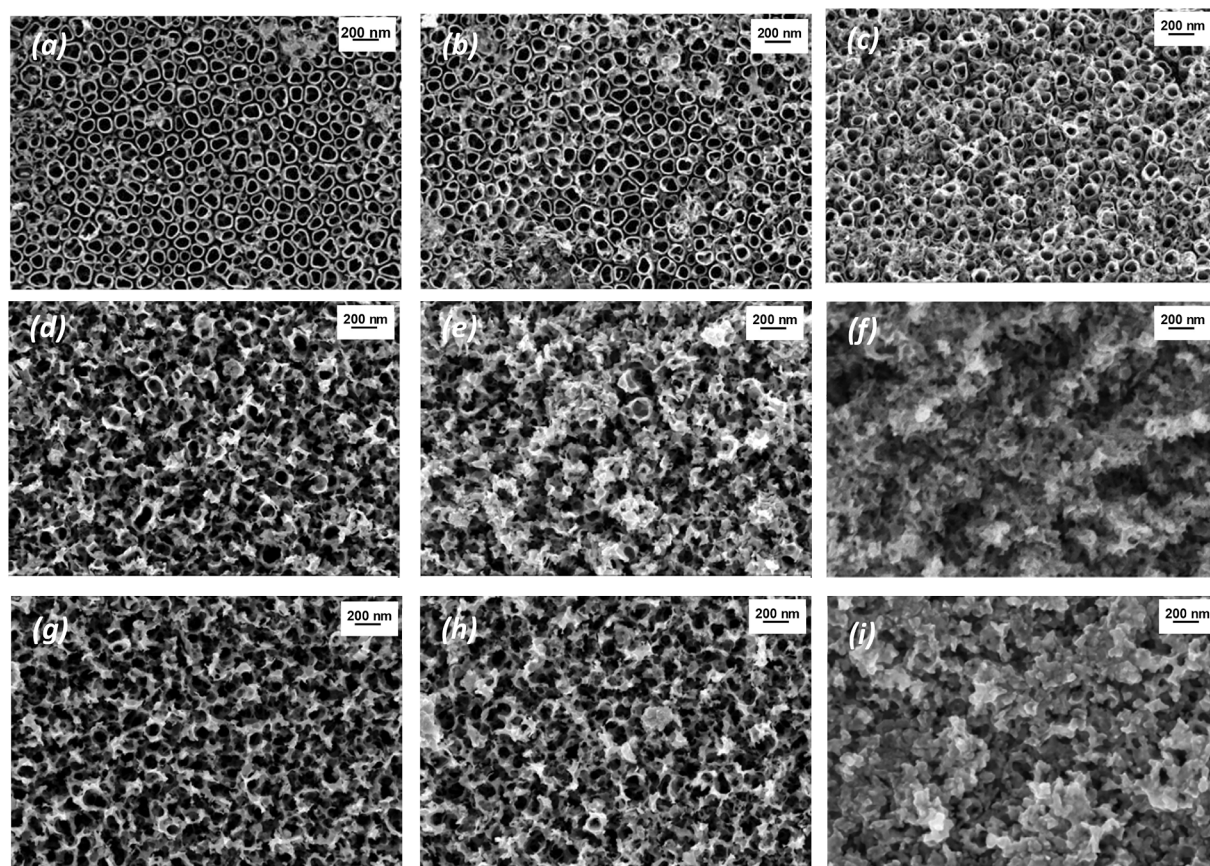


**Fig. 2.** SEM micrographs of the top of the coatings obtained at  $\text{NH}_4\text{F}$  different concentrations in the electrolyte. (a) G-0.06M-20V-2h-C; (b) G-0.15M-20V-2h-C; (c) G-0.27M-20V-2h-C; (d) G-0.06M-40V-2h-C; (e) G-0.15M-40V-2h-C; (f) G-0.27M-40V-2h-C; (g) G-0.06M-60V-2h-C; (h) G-0.15M-60V-2h-C; (i) G-0.27M-60V-2h-C.

40 kV and 50 mA, respectively. The UV-Vis diffuse reflectance spectra (DRS) of the samples were obtained at RT in air using an Ocean Optics DH-2000-BAL UV-Vis-NIR spectrophotometer equipped with an integrating sphere. The DRS data were used to obtain the bandgap of samples through Tauc plots ( $E_g$  was obtained by extrapolating to zero a linear fit to a plot of  $(kh\nu)^{1/2}$  against  $h\nu$ , as reported in reference (Murphy, 2007).

#### 2.4. Photocatalytic tests

A 0.4 mM  $\text{K}_2\text{Cr}_2\text{O}_7$  aqueous solution containing 1 mM EDTA was used for the photocatalytic tests. The initial pH was adjusted to 2 with perchloric acid. The photocatalyst samples were immersed into 10 mL of this solution contained in cylindrical reactors (45 mm diameter and 68 mm high) under magnetic stirring (Velp multistirrer 6), and six different samples were irradiated simultaneously using a BLV MHL404 UV lamp

( $\lambda > 250$  nm, maximum emission at 365 nm). Between the UV lamp and the reactor, a water filter and a glass filter were placed, to filter IR and UV wavelengths lower than 300 nm, respectively. The mean incident UV irradiance ( $E_0$ ) measured at 365 nm was  $3700 \mu\text{W cm}^{-2}$ . Prior to irradiation, the solutions were kept in the dark with continuous stirring for 30 min, to ensure the adsorption equilibrium between the pollutant and the photocatalyst. No significant changes in Cr(VI) concentration were observed after this dark period. 50  $\mu\text{L}$  samples were taken each hour and diluted in 3 mL of water for analysis. Changes in Cr(VI) concentration were spectrophotometrically monitored through the DFC method at 540 nm (ASTM D1687-12, 2012) using a Shimadzu UV-Vis spectrophotometer, model UV2550. To evaluate the homogeneous photochemical reduction of Cr(VI), the model pollutant was irradiated in the absence of  $\text{TiO}_2$  (blank experiment). An error of 5% was assumed for the photocatalytic experiments. The experimental points were fitted with the Origin 8.0 software, with reduced  $\chi^2$  as the iteration ending criterion.

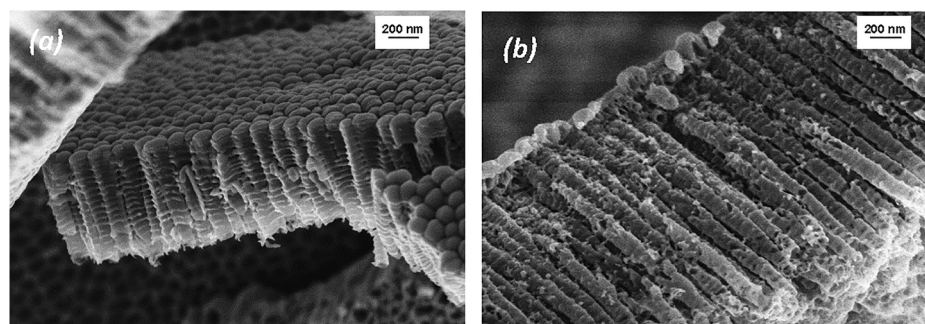


**Fig. 3.** SEM micrographs of the side view of the coatings obtained at  $\text{NH}_4\text{F}$  different concentrations: (a) G-0.06M-20V-2h-C; (b) G-0.27M-20V-2h-C.

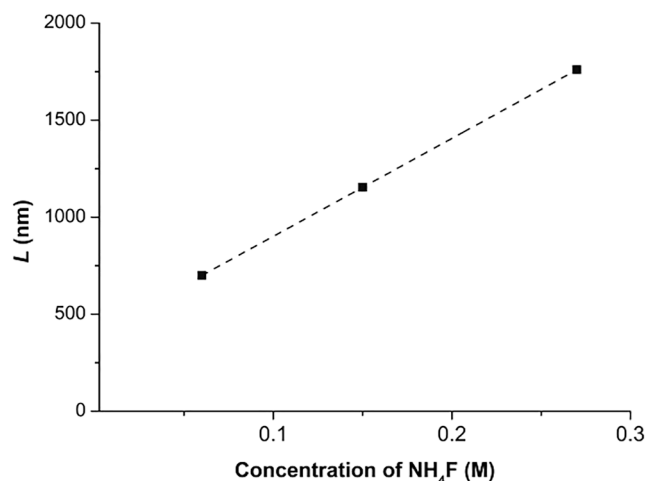


Fig. 4. Relationship between the length of the nanotubes and the concentration of NH<sub>4</sub>F in the electrolyte.

### 3. Results and discussion

#### 3.1. Characterization of the coatings

##### 3.1.1. SEM images: Morphology

**3.1.1.1. Influence of the NH<sub>4</sub>F concentration and anodizing voltage on the formation of the nanotubes.** The films obtained with different applied voltages during the anodizing of Ti plates using NH<sub>4</sub>F as the electrolyte in glycerol during two hours are shown in Fig. 2. As it can be observed, different morphologies of the films are obtained, but only those produced at 20 V show nanotubular structures (Fig. 2 (a), (b), and (c), top view of the material). In such cases, the nanotubes have a nearly circular top section, shown in light grey color with a dark grey or black interior. However, Maulidiyah et al. showed nanotubes in glycerol-based electrolytes at 25 V (Maulidiyah et al., 2017). The films obtained at higher voltages for any electrolyte concentration have a sponge-like shape, assumed to be the result of the collapse of the nanotubular structure

during the anodization (Regonini et al., 2013).

With respect to the nanotubular structures from Fig. 2 (a) to (c), it is observed that increasing the NH<sub>4</sub>F concentration from 0.06 M to 0.27 M does not change the diameters of the nanotubes; however, the homogeneity of the structure strongly deteriorates, particularly the wall structure. For high voltages (40 and 60 V), the effect of increasing the NH<sub>4</sub>F concentration also strongly deteriorates the general aspect of the films, being transformed from the nanotubes observed at 20 V to a completely amorphous structure at 60 V (Fig. 2 (f) and (i)).

The side view of the nanotubes shows a significant length increase with the increase of the NH<sub>4</sub>F concentration (Fig. 3 and Table 2), which could be attributed to a faster oxidation velocity as suggested in the literature (Alivov et al., 2009). On the other hand, in the range of experimental conditions of the present research, the length of the nanotubes linearly increases with the NH<sub>4</sub>F concentration in the electrolyte ( $R^2 = 1$ ) (Fig. 4).

Other micrographs corresponding to samples with different surface treatments are included in the SI as Fig. S3.

The effect of the applied voltage, in the range from 10 V to 60 V, can be clearly observed in Fig. 5 for 0.27 M NH<sub>4</sub>F. It can be seen that only at 20 V a regular nanotubular structure is produced. In Fig. 5 (a), the red dotted circles indicate that the materials obtained at 10 V are nanotubes. In addition, it can be observed an irregular film surface grown on the nanotubes, named nanograss (Regonini et al., 2012). In the regular nanotubular structure (Fig. 5 (b)), almost no nanograss structures are present. In Fig. 5 (c), a film produced at 30 V, the nanotubes that are present are not clearly defined, and the structure is highly irregular, indicating that, at this voltage, the nanotubes start to collapse. In Fig. 5 (d) to (f), although there is no evidence of nanotubes, some pseudotubular structures can however be seen. Finally, the nanotubes produced at 20 V have a higher diameter than those produced at 10 V (Table 2).

On the other hand, when higher voltages up to 100 V were applied to samples prepared with 0.06 and 0.15 M NH<sub>4</sub>F, no nanotubes were observed, as opposed to that reported by Alivov et al., who observed nanotubes up to 160 V using 0.2% (0.06 M) NH<sub>4</sub>F concentration in glycerol with no water addition (Regonini et al., 2012).

##### 3.1.1.2. Influence of the anodizing time on the formation of the nanotubes.

The anodizing time has a direct effect on the length of the nanotubes and

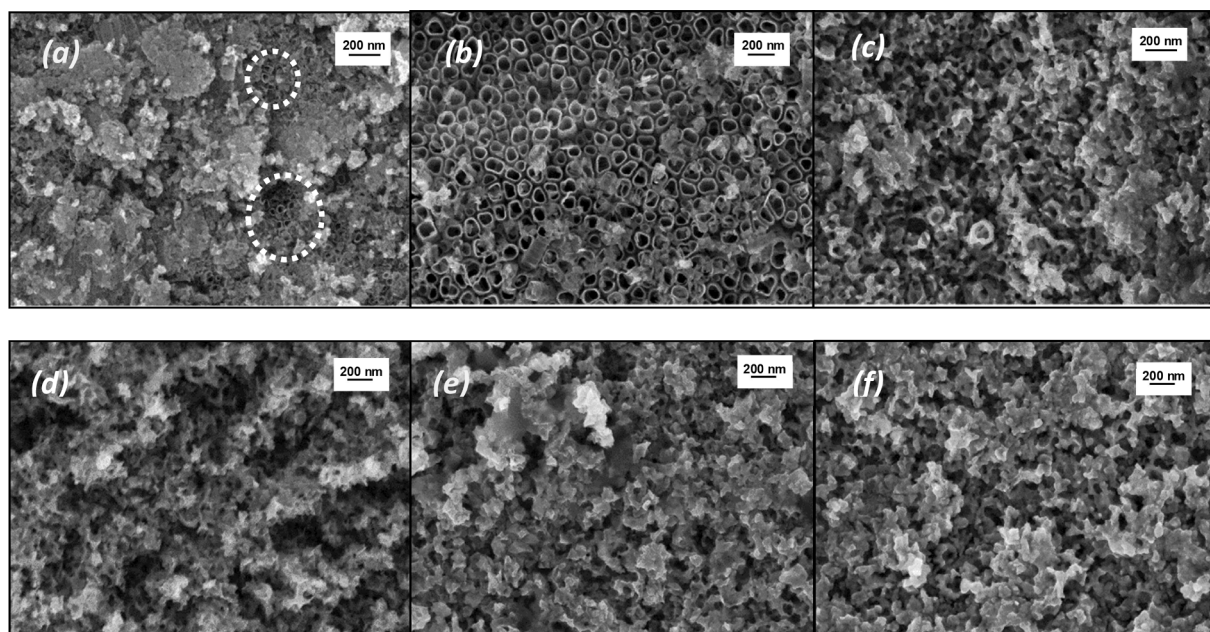
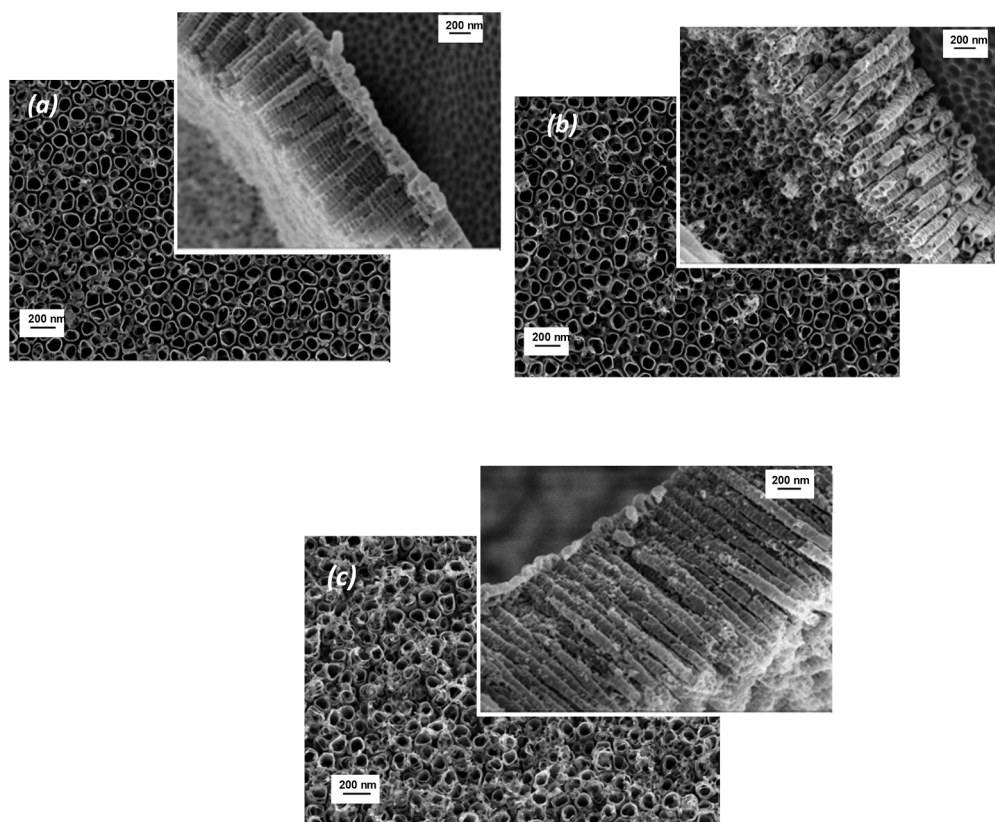
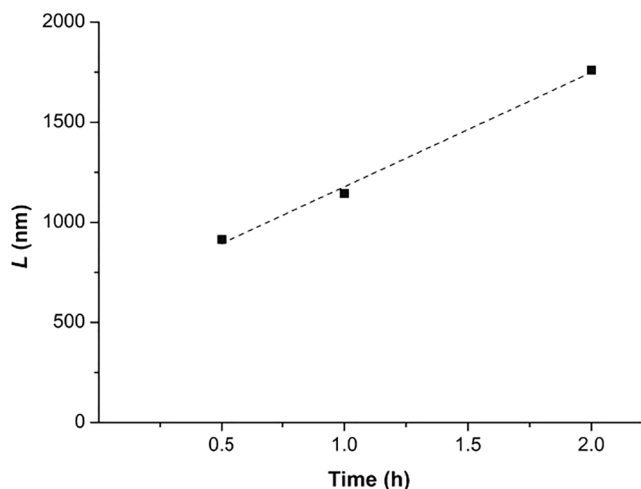


Fig. 5. SEM micrographs of the top of the coatings obtained at different voltages. (a) G-0.27M-10V-2h-P; (b) G-0.27M-20V-2h-P; (c) G-0.27M-30V-2h-P; (d) G-0.27M-40V-2h-P; (e) G-0.27M-50V-2h-P; (f) G-0.27M-60V-2h-P.



**Fig. 6.** SEM micrographs of the top and lateral views of the coatings obtained at different anodizing times (a) G-0.27M-20V-0.5 h-C; (b) G-0.27M-20V-1h-C; (c) G-0.27M-20V-2h-C.



**Fig. 7.** Relationship between the length of the nanotubes and the anodizing time.

an opposite effect on the uniformity and quality of the nanotube array. In Fig. 6, the top and lateral views of the SEM micrographs of the nanotubes obtained in a 0.27 M electrolyte, at 20 V and during 0.5, 1, and 2 h are shown. It can be observed that the length of the nanotubes increases as time increases, in agreement with the results reported in the literature (Regonini et al., 2013).

On the other hand, the top views of the materials shown in Fig. 6 indicate a loss of the uniformity of the nanotubes as the anodizing time increases, attributable to a distortion due to the fact that the nanotubes adopt a conical shape, keeping their internal diameter constant and with thinner walls (Valota et al., 2009). However, once the nanotubes are

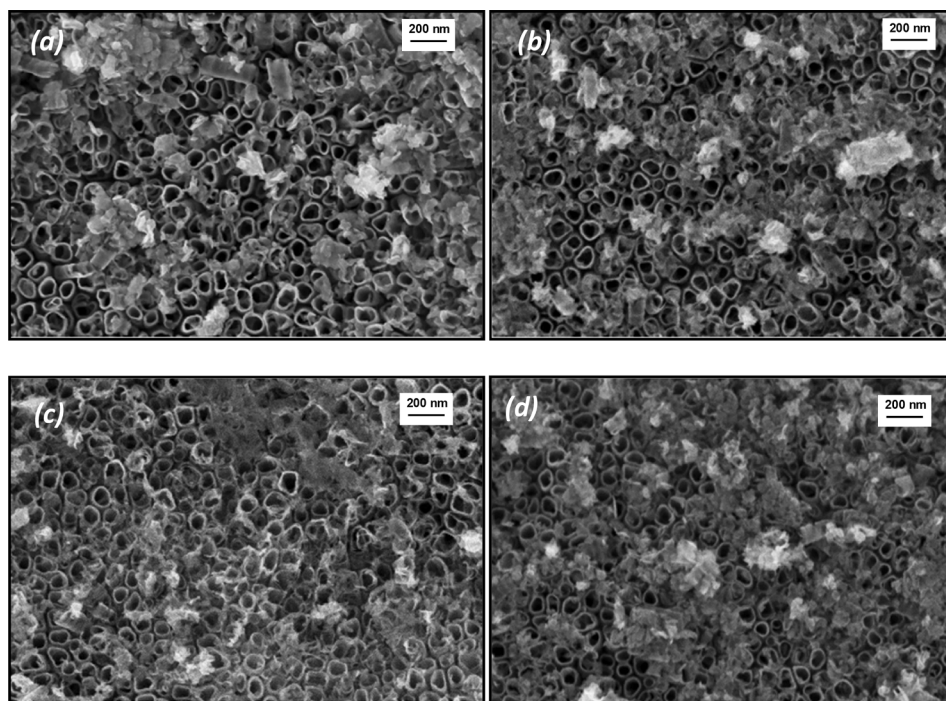
formed, they are very stable and maintain the same regularity.

Fig. 7 shows that, in the range of the studied experimental conditions, the length of the nanotubes increases quite linearly with anodizing time (571 nm/h;  $R^2 > 0.99$ ).

In order to explore the possibility of the formation of nanotubes under different conditions than those established in the previous section, samples were anodized during 1 and 4 h using electrolyte concentrations of 0.06 and 0.15 M of  $\text{NH}_4\text{F}$  at 40 and 60 V. No nanotubular arrays were produced in any of such conditions (see the SI, Section S3).

From the results described in Sections 3.1.1.1 and 3.1.1.2, it may be concluded that the anodizing time does not affect the array, i.e., once the nanotubes are formed, they remain stable with time. On the other hand, the anodizing voltage becomes the critical parameter considering that uniform arrays were obtained only at 20 V.

**3.1.1.3. Influence of the substrate preparation on the formation of the nanotubes.** The arrays of nanotubes produced on titanium surfaces with different finishing are shown in Fig. 8. They correspond to top SEM views obtained using 0.27 M of  $\text{NH}_4\text{F}$  at 20 V during 2 h. The preparation of the surface includes polishing up to 1  $\mu\text{m}$  diamond paste (P, Fig. 8 (a)), continuing with chemical pickling (C, Fig. 8 (b)), then degreasing (D, Fig. 8 (c)) and finally roughing (R, Fig. 8 (d)). Comparing the micrographs, it can be concluded that the surface finishing has no effect on the morphology of the nanotubes, i.e., it does not affect either the internal diameter or the wall thickness. Nevertheless, the difference in the appearance of the nanotubes produced with the R and D finishings with respect to those obtained with the P and C finishings could be due to an incomplete elimination of the natural oxide in the R and D, which may affect the nanotube formation at the beginning of the anodization process and continues afterwards.



**Fig. 8.** SEM micrographs of the top of the coatings obtained with different preparations of the surface of the substrate. (a) G-0.27M-20V-2h-P; (b) G-0.27M-20V-2h-C; (c) G-0.27M-20V-2h-D; (d) G-0.27M-20V-2h-R.

### 3.1.2. XRD patterns: Crystalline structures

The XRD patterns of samples are shown in Fig. 9 (a), (b) and (c). In each figure, the normalized patterns are grouped in order to compare the structure obtained as a function of one of the following anodizing parameters: three different  $\text{NH}_4\text{F}$  concentrations (Fig. 9 (a)), anodizing time (Fig. 9 (b)), and substrate preparation (Fig. 9 (c)).

The first observation is that in the spectrum of G-0.27M-20V-2h-C (Fig. 9 (a)), only diffraction peaks of the Ti substrate can be seen, indicating that the nanotubes without TT are amorphous.

The XRD spectrum of thermally treated samples mainly shows the anatase phase (1 0 1), which is formed on the nanotube walls. The small rutile peaks (1 1 0) can be probably attributed to the thermal oxidation of the Ti substrate (Grimes and Mor, 2009; Varghese et al., 2003).

In Fig. 9 (a), it can be clearly seen that, as the concentration of  $\text{NH}_4\text{F}$  increases, the relative anatase peak also increases in intensity. A similar observation can be made by comparing the height of the anatase peak in Fig. 9 (b), which increases with the anodizing time. Both effects are due to the increase of the length of the nanotubes, as shown in Table 2 and discussed in the previous sections. On the other hand, Fig. 9 (c) shows that the anatase phase appears in all cases, independently of the substrate preparation.

The amount of the anatase phase is not directly shown in the diffractograms since the intensity of the peaks is normalized. However, the absolute value of the anatase peak (1 0 1) in the polished sample (P) is 60% higher than the corresponding peak of the chemical pickling sample (C) (see the SI, Section S4). This result can also be related to the length of the nanotubes since, in the C, R, and D samples (Table 2), this length is around 1760 nm while, in the case of the P sample, it could be larger. Therefore, in all cases shown in Fig. 9, the larger amount of the anatase phase is related to the larger nanotubes.

From these results, it can be concluded that the TT is effective in crystallizing the anatase phase in  $\text{TiO}_2$  nanotubes.

### 3.1.3. Diffuse reflectance spectra: Calculation of the bandgap values of the samples

The bandgap values of the samples were obtained by following the procedure described in Section 2.3, and they are listed in Table 2. In all

cases, bandgaps of  $\sim 3.3$  eV were obtained, i.e., slightly higher than the reported values for anatase (3.2 eV) (Grimes and Mor, 2009). This higher value could be due to the effect of mirror reflections from the substrate on the spectra, resulting from the relatively small thickness of the films; it can also be due to a quantum confinement from the nanotube walls (Vera et al., 2018) (Table 2). It is noted that the anodizing conditions do not affect the bandgap value.

## 3.2. Cr(VI)/EDTA photocatalytic experiments with the new photocatalysts

### 3.2.1. Photocatalytic efficiency

The efficiency of the photocatalytic activity of the nanotubes were determined applying the procedure described in Section 2.4 on the reduction of Cr(VI) in the presence of EDTA ( $[\text{Cr(VI)}]_0 = 0.8$  mM;  $[\text{EDTA}]/[\text{Cr(VI)}] = 1.25$ ; pH 2;  $E_0 = 3700 \mu\text{W cm}^{-2}$ ). The results for the different nanotube samples are presented in Fig. 10 where the Cr(VI) concentration during the experiments (C) is normalized with respect to the initial Cr(VI) concentration ( $C_0$ ) and plotted as a function of the irradiation time; a comparison with the system in the absence of photocatalyst (i.e., blank test) is also shown. The results are presented in different figures to analyze the effect on the efficiency due to the  $\text{NH}_4\text{F}$  concentration (Fig. 10 (a)), anodizing time (Fig. 10 (b)), and substrate preparation (Fig. 10 (c)). In all cases, the experimental points were fitted using the following equation:

$$\frac{C}{C_0} = e^{-k_1 \times t} \quad (1)$$

where  $k_1$  is the pseudo-first-order kinetic constant. The fittings were very good in all cases ( $R^2 > 0.98$ ) showing that this kinetics adjusts very well to the results with photocatalysts with large surface area as in the present case, indicating that the surfaces of the nanotubes are not saturated with adsorbed chromium. The reduction rate of Cr(VI) depends on its concentration, similarly to that observed in experiments of homogeneous photocatalysis (Vera et al., 2018). In all cases, Cr(VI) reduction was faster in the presence of the photocatalyst than in the

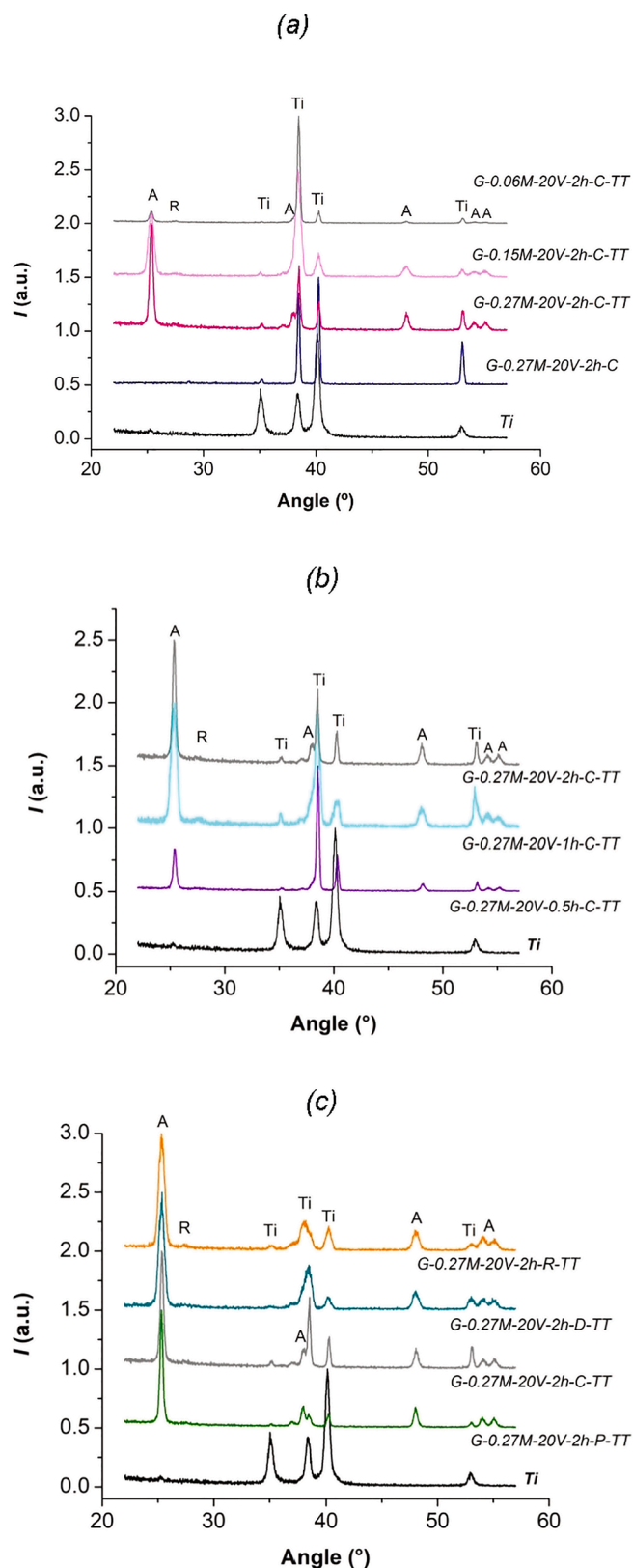


Fig. 9. XRD patterns of samples of nanotubes grouped by: (a)  $\text{NH}_4\text{F}$  concentration, (b) time, (c) substrate preparation. A = anatase, R = rutile, Ti = titanium.

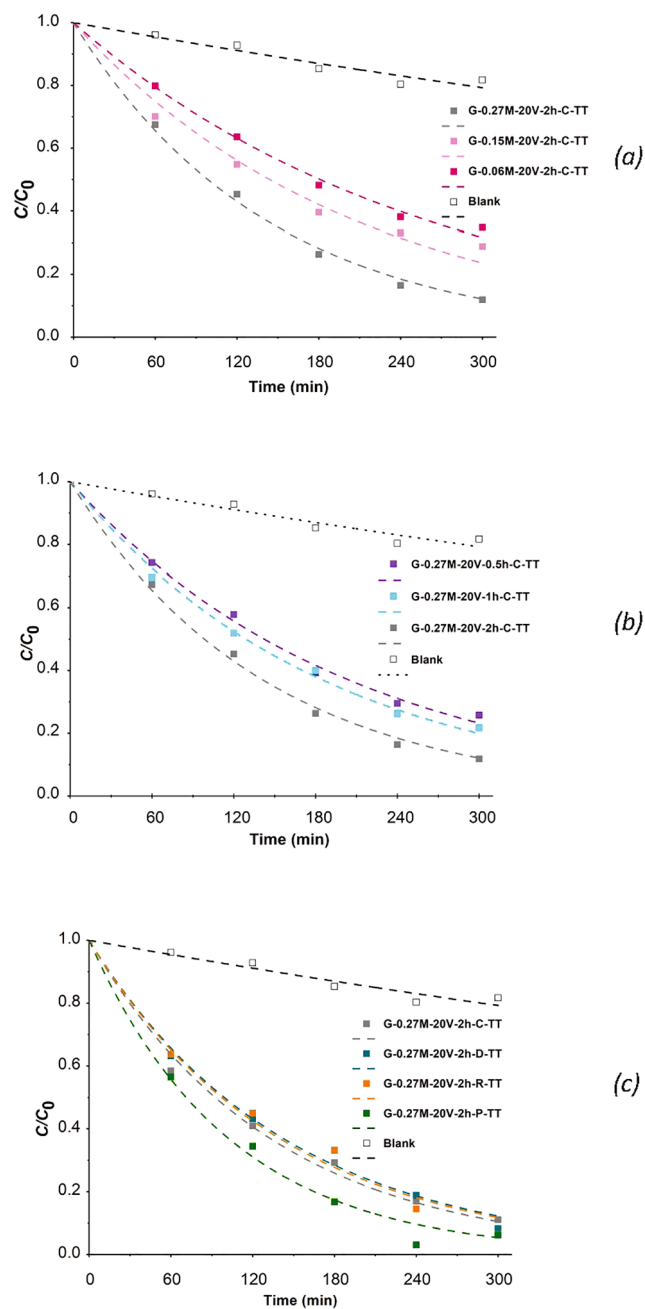


Fig. 10. Evolution profile of normalized Cr(VI) concentration ( $C/C_0$ ) in photocatalytic experiments of Cr(VI) transformation in the presence of EDTA under UV irradiation. Influence on the photocatalytic activity of: (a)  $\text{NH}_4\text{F}$  concentration; (b) time; (c) substrate preparation. Conditions:  $[\text{Cr(VI)}]_0 = 0.8 \text{ mM}$ ;  $[\text{EDTA}]/[\text{Cr(VI)}] = 1.25$ ; pH 2;  $E_0 = 3700 \mu\text{W cm}^{-2}$ . The dashed lines are the fittings of the experimental points with Eq. (1).

blank experiment.

The values of the kinetic parameter  $k_1$  for each of the twelve samples and the blank are listed in Table 3. It is noted that a faster kinetics is obtained in samples anodized at higher  $\text{NH}_4\text{F}$  concentrations (Fig. 10 (a)), and for longer times (Fig. 10 (b)), meaning longer nanotubes and samples with a greater amount of anatase crystals (Masahashi et al., 2009). This is supported by the result of the lower efficiency of the G-0.06M-20V-2h-C-TT sample, which has the shortest nanotubes (sample 1 in Table 2 and sample 9 in Table 3). Moreover, higher concentration and longer anodization time should be tested in the future in order to explore the optimum synthesis condition able to produce more efficient

**Table 3**

Pseudo-first-order kinetic constants ( $k_1$ ) and percentage of Cr(VI) removal in the presence of EDTA at 300 min, extracted from Fig. 10.

Sample	$k_1 \times 10^{-3} \text{ (min}^{-1}\text{)}$	$R^2$	%Cr(VI) removal
1	Blank	0.77	18.3
2	G-0.27M-20V-2h-C-TT	7.50	88.9
3	G-0.27M-20V-2h-P-TT	9.75	93.8
4	G-0.27M-20V-2h-D-TT	6.99	91.8
5	G-0.27M-20V-2h-R-TT	7.13	93.7
6	G-0.27M-20 V-1 h-C-TT	5.37	78.2
7	G-0.27M-20 V-0.5 h-C-TT	4.87	74.2
8	G-0.15M-20V-2h-C-TT	4.82	71.2
9	G-0.06M-20V-2h-C-TT	3.83	65.3
10	G-0.27M-10V-2h-P-TT	4.99	81.1
11	G-0.27M-30V-2h-P-TT	3.25	63.3
12	G-0.27M-20V-2h-C-TT-d	7.03	88.1
13	G-0.27M-20V-2h-C-TT-r	2.56	56.1

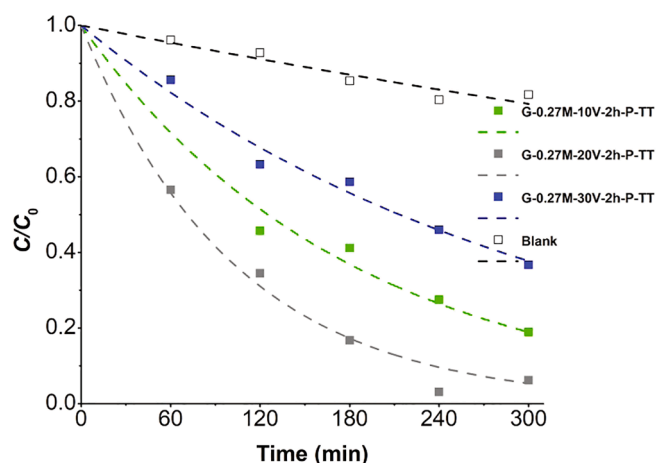


Fig. 11. Evolution profile of normalized Cr(VI) concentration ( $C/C_0$ ) in photocatalytic experiments of Cr(VI) transformation in the presence of EDTA under UV irradiation. Influence of the type of nanostructure obtained at different voltages on the photocatalytic activity. Conditions:  $[\text{Cr(VI)}]_0 = 0.8 \text{ mM}$ ;  $[\text{EDTA}]/[\text{Cr(VI)}] = 1.25$ ; pH 2;  $E_0 = 3700 \mu\text{W cm}^{-2}$ . The dashed lines are the fittings of the experimental points with Eq. (1).

photocatalysts.

On the other hand, Fig. 10 (c) shows that the substrate preparation method has minor effects on the photoactivity of the films, as expected since the process is controlled by the amount of anatase crystals. Transformations were around 90%, the largest value of 93.8% corresponding to the polished sample. This is an important result from a technological point of view since the pickling technique for the preparation of the substrate surface is simple and suitable for production at a larger scale. Moreover, this technique can be employed for non-flat surfaces like tubes, rings, and others.

The effect of the anodizing voltage on the photocatalytic efficiency is presented in Fig. 11. The best efficiency is achieved in the case of the nanotubes produced at 20 V, followed by the sample produced at 10 V and that produced at 30 V. The nanotube array of the sample produced at 20 V is very uniform, long, and without nanograss, which are favorable properties for a good photocatalytic efficiency. The sample obtained at 10 V has shorter nanotubes and is covered by nanograss. The presence of the nanograss structure is associated with the slimming of the nanotube walls, which could produce their bending and collapse at a long anodizing time (Yasuda and Schmuki, 2007; So et al., 2012). This may alter the photocatalytic efficiency by shadowing the nanotubes for the incidence of the UV irradiation. The sample produced at 30 V, in which the nanotubes are longer but very inhomogeneous, presents the lowest efficiency.

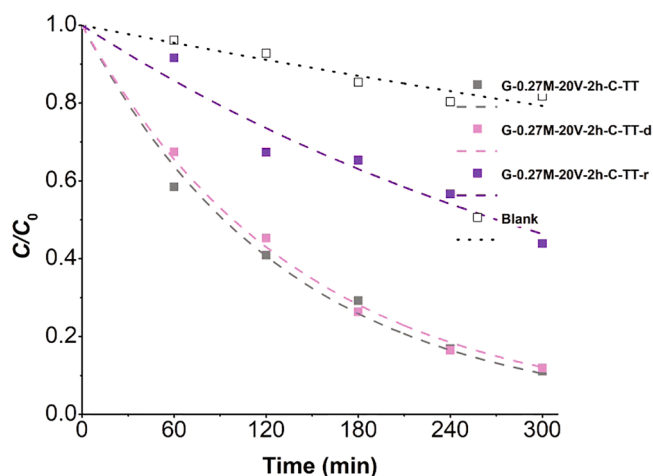


Fig. 12. Evolution profile of normalized Cr(VI) concentration ( $C/C_0$ ) in the photocatalytic experiments of Cr(VI) transformation in the presence of EDTA under UV irradiation performed with two samples prepared in a similar way and with a reused sample. Conditions:  $[\text{Cr(VI)}]_0 = 0.8 \text{ mM}$ ;  $[\text{EDTA}]/[\text{Cr(VI)}] = 1.25$ ; pH 2;  $E_0 = 3700 \mu\text{W cm}^{-2}$ . The dashed lines are the fittings of the experimental points with Eq. (1).

### 3.2.2. Reproducibility and reuse of the photocatalysts

For the use of the present photocatalysts in the construction of pilot and plant photoreactors for water treatment, they must show at least two important behavior characteristics with respect to the efficiency: 1) they should change the efficiency within limits of tolerance when produced by the same technique (reproducibility), and 2) they should show similar efficiencies with the repeated use (reuse).

In order to investigate these two technological aspects, two samples of “G-0.27M-20V-2h-C-TT” were produced under the same conditions in different batches. This sample was chosen not for its efficiency but because of the surface treatment (chemical pickling), which is the simplest method and requires less time (only 2 min) and no previous preparation and, more importantly, it may be used for different surface geometries. These advantages would greatly compensate for a little lower efficiency, permitting the design and construction of photoreactors with non-flat geometries.

The original sample and the second one (duplicate, labeled as “d”), were tested to assess anodization reproducibility. For testing the reuse, the original sample was evaluated a second time and the corresponding curve was labeled as “r” in Fig. 12.

Fig. 12 shows that the original sample and its duplicate have an almost identical behavior, showing that the production technique is reproducible. On the other hand, the efficiency of the Cr(VI) reduction decreased by approximately 36% after the first reuse (see also Table 2). The reduction in the efficiency of the catalyst after reuse could be attributed to the saturation of the photocatalyst surface by adsorption of Cr(III) species, which reduces the effective active surface. This last result indicates that the reutilization of the photocatalyst would require a reactivation process that must be designed and applied before its reuse (Salaeh et al., 2017). The reactivation treatments will be investigated in next experiments. Some possibilities are the cleaning of the sample with hydrogen peroxide (Gandhi et al., 2012), which has been demonstrated to be successful for  $\text{TiO}_2$  particle suspensions, the cleaning with solvents followed by heat treatment (Salaeh et al., 2017), or a combination of these treatments adjusting sequence, concentration, time of cleaning and temperature in the last case. These experiments and the evaluation of the photocatalytic efficiency are underway.

## 4. Conclusions

$\text{TiO}_2$  films were produced by anodizing Ti substrates in electrolytes

prepared with glycerol-NH<sub>4</sub>F-H<sub>2</sub>O. The objective was to obtain TiO<sub>2</sub> nanotube arrays with the best possible efficiency for heterogeneous photocatalysts to be used for water decontamination in photoreactors at pilot and plant scales. Several parameters and substrate preparations were assessed experimentally, namely NH<sub>4</sub>F concentration, applied voltage, anodizing time, and different surface finishing. To increase the amount of anatase crystals, the films were thermally treated.

From the results of anodization it can be concluded that, for a good photocatalytic efficiency, the nanotube arrays must present the largest length and be homogeneous in size and morphology. The best arrays were obtained by using the following anodizing conditions: 0.27 M NH<sub>4</sub>F concentration, 20 V during 2 h, followed by a thermal treatment. All the others conditions produce non-uniform arrays, amorphous morphology, nanograss, and other defects that reduce the efficiency.

The best efficiency for reducing Cr(VI) in the presence of EDTA was 93.8% after 5 h of UV radiation and was obtained with the G-0.27M-20V-2h-P-TT sample. This was attributed to a good anatase crystallinity and the high contact area provided by the longest nanotubes. Moreover, higher concentrations and longer anodization times will be tested in the future in order to explore the optimum synthesis condition able to produce more efficient photocatalysts.

The applied fabrication technique results in reproducible nanotube arrays in size, morphology, and also in photocatalytic efficiency.

#### Declaration of Competing Interest

The authors declare that they have no known competing financial interests or personal relationships that could have appeared to influence the work reported in this paper.

#### Acknowledgments

The authors would like to thank CONICET and Agencia Nacional de Promoción Científica y Tecnológica (ANPCyT) from Argentina, PICT-2017-2133 and PICT-2015-0208 projects. The authors thank Dr. Paula Angelomé from the Nanomaterials Chemistry Group of Gerencia Química of Centro Atómico Constituyentes, Comisión Nacional de Energía Atómica and Eng. Cristian Cegelski from the DRX Laboratory of Instituto de Materiales de Misiones (IMAM, CONICET-UNaM) for measurements of the samples.

#### Appendix A. Supplementary data

Supplementary data to this article can be found online at <https://doi.org/10.1016/j.enmm.2021.100537>.

#### References

- Albu, S., Kim, D., Schmuki, P., 2008. Growth of aligned TiO<sub>2</sub> bamboo-type nanotubes and highly ordered nanolace. *Angew. Chem.* 120 (10), 1942–1945.
- Alivov, Y., Pandikunta, M., Nikishin, S., Fan, Z.Y., 2009. The anodization voltage influence on the properties of TiO<sub>2</sub> nanotubes grown by electrochemical oxidation. *Nanotechnol.* 20 (22), 225602. <https://doi.org/10.1088/0957-4484/20/22/225602>.
- ASTM D1687-12. Standard Test Methods for Chromium in Water. A Photometric Diphenyl-carbohydrazide (2012).
- Barbero, N., Vione, D., 2016. Why Dyes Should Not Be Used to Test the Photocatalytic Activity of Semiconductor Oxides. *Environ. Sci. Technol.* 50 (5), 2130–2131.
- Chromium Compounds in Ullmann's encyclopedia of industrial chemistry (2005). 4424–4459.
- Gandhi, V.G., Mishra, M.K., Joshi, P.A., 2012. A study on deactivation and regeneration of titanium dioxide during photocatalytic degradation of phthalic acid. *J. Ind. Eng. Chem.* 18 (6), 1902–1907.
- Gong, D., Grimes, C.A., Varghese, O.K., Hu, W., Singh, R.S., Chen, Z., Dickey, E.C., 2001. Titanium oxide nanotube arrays prepared by anodic oxidation. *J. Mater. Res.* 16 (12), 3331–3334.

- Grimes, C.A., Mor, G.K., 2009. TiO<sub>2</sub> nanotube arrays: synthesis, properties, and applications. Springer Science & Business Media.
- Macak, J.M., Tsuchiya, H., Ghicov, A., Yasuda, K., Hahn, R., Bauer, S., Schmuki, P., 2007. TiO<sub>2</sub> nanotubes: self-organized electrochemical formation, properties and applications. *Curr. Opin. Solid State Mater. Sci.* 11 (1), 3–18.
- Malato, S., Fernandez-Ibanez, P., Maldonado, M.I., Blanco, J., Gernjak, W., 2009. Decontamination and disinfection of water by solar photocatalysis: recent overview and trends. *Catal. Today* 147 (1), 1–59.
- Masahashi, N., Mizukoshi, Y., Semboshi, S., Ohtsu, N., 2009. Enhanced photocatalytic activity of rutile TiO<sub>2</sub> prepared by anodic oxidation in a high concentration sulfuric acid electrolyte. *Appl. Catal. B* 90 (1–2), 255–261.
- Maulidiyah, M., Azis, T., Nurwahidah, A.T., Wibowo, D., Nurdin, M., 2017. Photoelectrocatalyst of Fe co-doped N-TiO<sub>2</sub>/Ti nanotubes: pesticide degradation of thiamethoxam under UV-visible lights. *Environ. Nanotechnol. Monit. Manage.* 8, 103–111.
- Murphy, A., 2007. Band-gap determination from diffuse reflectance measurements of semiconductor films, and application to photoelectrochemical water-splitting. *Sol. Energy Mater. Sol. Cells* 91 (14), 1326–1337.
- Nakata, K., Fujishima, A., 2012. TiO<sub>2</sub> photocatalysis: Design and applications. *J. Photochem. Photobiol., C* 13 (3), 169–189.
- Ollis, D., Silva, C.G., Faria, J., 2015. Simultaneous photochemical and photocatalyzed liquid phase reactions: Dye decolorization kinetics. *Catal. Today* 240, 80–85.
- Pang, Y.L., Lim, S., Ong, H.C., Chong, W.T., 2014. A critical review on the recent progress of synthesizing techniques and fabrication of TiO<sub>2</sub>-based nanotubes photocatalysts. *Appl. Catal. A* 481, 127–142.
- Pichat, P., 2014. Are TiO<sub>2</sub> nanotubes worth using in photocatalytic purification of air and water? *Mol. Phys.* 19 (9), 15075–15087.
- Regonini, D., Satka, A., Jaroenworuluck, A., Allsopp, D.W.E., Bowen, C.R., Stevens, R., 2012. Factors influencing surface morphology of anodized TiO<sub>2</sub> nanotubes. *Electrochim. Acta* 74, 244–253.
- Regonini, D., Bowen, C.R., Jaroenworuluck, A., Stevens, R., 2013. A review of growth mechanism, structure and crystallinity of anodized TiO<sub>2</sub> nanotubes. *Mater. Sci. Eng., R* 74 (12), 377–406.
- Robert, D., Keller, N., Keller, V., 2013. Immobilization of a semiconductor photocatalyst on solid supports: methods, materials, and applications. *Photocatal. Water Purification* 145–178.
- Rudnev, V.S., Vasil'eva, M.S., Lukiyanchuk, I.V., Kuryavyi, V.G., 2004. On the surface structure of coatings formed by anodic spark method. *Prot. Met.* 40 (4), 352–357.
- Salaeh, S., Kovacic, M., Kosir, D., Kusic, H., Stangar, U.L., Dionysiou, D., Bozic, A.L., 2017. Reuse of TiO<sub>2</sub>-based catalyst for solar driven water treatment: thermal and chemical reactivation. *J. Photochem. Photobiol., A* 333, 117–129.
- Schneider, C.A., Rasband, W.S., Eliceiri, K.W., 2012. NIH Image to ImageJ: 25 years of image analysis. *Nat. Methods* 9 (7), 671–675.
- So, S., Lee, K., Schmuki, P., 2012. Ultrafast growth of highly ordered anodic TiO<sub>2</sub> nanotubes in lactic acid electrolytes. *J. Am. Chem. Soc.* 134 (28), 11316–11318.
- Stodolny, M., Zagrodnik, R., Nowaczyk, G., Jurga, S., 2017. Size-controlled synthesis of anatase nanobrush structures with higher crystal density. *Mater. Res. Bull.* 94, 335–341.
- Traid, H.D., Vera, M.L., Ares, A.E., Litter, M.I., 2017. Advances on the synthesis of porous TiO<sub>2</sub> coatings by anodic spark oxidation. Photocatalytic reduction of Cr (VI). *Mater. Chem. Phys.* 191, 106–113.
- Valota, A., LeClere, D.J., Skeldon, P., Curioni, M., Hashimoto, T., Berger, S., Kunze, J., Schmuki, P., Thompson, G.E., 2009. Influence of water content on nanotubular anodic titania formed in fluoride/glycerol electrolytes. *Electrochim. Acta* 54 (18), 4321–4327.
- Varghese, O.K., Gong, D., Paulose, M., Grimes, C.G., Dickey, E.C., 2003. Crystallization and high-temperature structural stability of titanium oxide nanotube arrays. *J. Mater. Res.* 18, 156–165.
- Vera, M.L., Traid, H.D., Henrikson, E.R., Ares, A.E., Litter, M.I., 2018. Heterogeneous photocatalytic Cr(VI) reduction with short and long nanotubular TiO<sub>2</sub> coatings prepared by anodic oxidation. *Mater. Res. Bull.* 97, 150–157.
- Wang, W.Y., Chen, B.R., 2013. Characterization and photocatalytic activity of TiO<sub>2</sub> nanotube films prepared by anodization. *Int. J. Photoenergy* 1–13.
- Wang, W., Tao, J., Wang, T., Wang, L., 2007. Photocatalytic activity of porous TiO<sub>2</sub> films prepared by anodic oxidation. *Rare Met.* 26 (2), 136–141.
- Wang, Y., Wu, Y., Qin, Y., Xu, G., Hu, X., Cui, J., Zheng, H., Hong, Y.u., Zhang, X., 2011. Rapid anodic oxidation of highly ordered TiO<sub>2</sub> nanotube arrays. *J. Alloy. Compd.* 509 (14), L157–L160.
- Wang, Q., Yang, X., Wang, X., Huang, M., Hou, J., 2012. Synthesis of N-doped TiO<sub>2</sub> mesopore by solvothermal transformation of anodic TiO<sub>2</sub> nanotubes and enhanced photoelectrochemical performance. *Electrochim. Acta* 62, 158–162.
- Yan, X., Ohno, T., Nishijima, K., Abe, R., Ohtani, B., 2006. Is methylene blue an appropriate substrate for a photocatalytic activity test? A study with visible-light responsive titania. *Chem. Phys. Lett.* 429 (4–6), 606–610.
- Yasuda, K., Schmuki, P., 2007. Formation of Self-Organized Zirconium Titanate Nanotube Layers by Alloy Anodization. *Adv. Mater.* 19 (13), 1757–1760.
- Zeng, X., Gan, Y.X., Clark, E., Su, L., 2011. Amphiphilic and photocatalytic behaviors of TiO<sub>2</sub> nanotube arrays on Ti prepared via electrochemical oxidation. *J. Alloy. Compd.* 509 (24), L221–L227.